

Role of long cycles in excitable dynamics on graphs

Guadalupe C. Garcia,^{1,*} Annick Lesne,^{2,3} Claus C. Hilgetag,^{4,5} and Marc-Thorsten Hütt¹

¹*School of Engineering and Science, Jacobs University Bremen, D-28759 Bremen, Germany*

²*LPTMC, CNRS UMR 7600, Université Pierre et Marie Curie, Sorbonne Universités, 4 place Jussieu, F-75252, Paris, France*

³*IGMM, CNRS UMR 5535, Université de Montpellier, 1919 route de Mende, F-34293, Montpellier, France*

⁴*Department of Computational Neuroscience, University Medical Center Hamburg-Eppendorf, Hamburg University, D-20148 Hamburg, Germany*

⁵*Department of Health Sciences, Boston University, Boston, Massachusetts 02215, USA*

(Received 6 July 2014; published 10 November 2014)

Topological cycles in excitable networks can play an important role in maintaining the network activity. When properly activated, cycles act as dynamic pacemakers, sustaining the activity of the whole network. Most previous research has focused on the contributions of short cycles to network dynamics. Here, we identify the specific cycles that are used during different runs of activation in sparse random graphs, as a basis of characterizing the contribution of cycles of any length. Both simulation and a refined mean-field approach evidence a decrease in the cycle usage when the cycle length increases, reflecting a trade-off between long time for recovery after excitation and low vulnerability to out-of-phase external excitations. In spite of this statistical observation, we find that the successful usage of long cycles, though rare, has important functional consequences for sustaining network activity: The average cycle length is the main feature of the cycle length distribution that affects the average lifetime of activity in the network. Particularly, use of long, rather than short, cycles correlates with higher lifetime, and cutting shortcuts in long cycles tends to increase the average lifetime of the activity. Our findings, thus, emphasize the essential, previously underrated role of long cycles in sustaining network activity. On a more general level, the findings underline the importance of network topology, particularly cycle structure, for self-sustained network dynamics.

DOI: [10.1103/PhysRevE.90.052805](https://doi.org/10.1103/PhysRevE.90.052805)

PACS number(s): 89.75.Hc, 87.19.lj

I. INTRODUCTION

Several mechanisms have been proposed for generating self-sustained brain dynamics and brain rhythms [1]. Some of these mechanisms are associated with intrinsic dynamic features of the individual neurons and others with network properties, generated by topological features of the graph in which the activity propagates. A mechanism to produce persistent oscillatory activity in a network of excitable elements has been proposed in [2], where the characteristics of the oscillations are determined purely by the structure of the graph. This type of self-sustained activity is produced by the re-entrance of activity in a cycle, and can drive the whole network at a period set by the length of the cycle. We here explore this type of activity, focusing on cycles and their impact on self-sustained network activity.

Several studies have analyzed the impact of cycles on the dynamics of networks of excitable elements. For example, it was shown in [3] for integrate-and-fire neurons that a very low density of shortcuts in a ring (yielding a small-world network) is sufficient for generating persistent activity from a local stimulus through the re-injection of activity into previously excited domains. In [4,5], based on continuous dynamics, a method for identifying the drivers of activity was proposed, by selecting the so-called dominant phase-advanced driving (DPAD) links, in order to unmask the self-organized structures supporting self-sustained activity. Others [6,7] also identified pacemaker loops and analyzed features of the oscillating states and their associated driving loops.

Most evidence on cycle usage so far, however, is indirect, as it is challenging to disentangle different topological contributions to the network dynamics. Here we use a highly generic discrete-state model of excitable dynamics which allows us to clearly define the usage of a cycle. The use of discrete dynamical models to explore relationships between network architecture and dynamics has previously provided key insights into the functions of complex networks, for example, Boolean models for gene regulatory networks [8] and “susceptible-infected-recovered” (SIR) and “susceptible-infected-susceptible” (SIS) models for epidemic diseases in social networks [9]. More generally, cellular automata (CA) models have been used in a vast number of investigations to explore the emergence of complex patterns from simple dynamic rules. Originally defined on regular lattices [10], they have also been studied on more complex topologies [11–13] and in noisy environments [14,15]. The principal goal of investigating CA on graphs is to explore the relationship between network architecture and dynamics from the perspective of pattern formation. Also for CA on graphs, the Wolfram classes [10,16] are a helpful and established means of characterizing observed dynamic behaviors (see, e.g., [12]).

The main purpose of this paper is to analyze the contribution of topological cycles to self-sustained activity in a network of excitable elements. To achieve this goal, we developed an algorithm to detect successfully used cycles in sparse Erdős-Rényi (ER) random graphs [17]. We worked with a basic model of excitable dynamics, a three-state CA, that allowed us to disentangle contributions from topology and the intrinsic dynamics of the node elements to self-sustained network activity.

Qualitatively speaking, the embedding of a cycle in the network perturbs the systematic “pacemaker” function that

*g.garcia@jacobs-university.de

this cycle would have in isolation. Such perturbations have a stronger effect with increasing cycle length, due to the associated increase of the number of external links through which out-of-phase excitations may enter the cycle. At the same time, however, the usage of cycles may also increase with cycle length, due to a longer cycling time available for refractory nodes after a first round of excitation. Due to the interplay of these conflicting influences, it is not *a priori* clear that short cycles dominate in their contribution to self-sustained network activity. Here we show that long cycles, indeed, are of relevance for maintaining excitable dynamics on graphs.

We first demonstrate that the excitable model allows us, due to its discrete nature, to understand the statistical properties of different regimes of cycle usage, and on this basis show how the average cycle length of a graph is a key feature for predicting the sustainability of a network. Finally, we reveal the role of shortcuts in long cycles with respect to the lifetime of sustained activity.

II. MATERIAL AND METHODS

A. Dynamic model

The dynamic model employed in this study consists of a three-state CA on the network. Each node can be in three discrete states: susceptible S , excited E , and refractory R . The node states are updated synchronously in discrete time steps according to a set of rules: (1) a susceptible node S becomes an excited node E when a directly linked neighbor is in the excited state; (2) an excited node E enters the refractory state R ; (3) a node regenerates with recovery probability p . The parameter p determines the average refractory time ($1/p$) of a node. For p close to one, the system is almost deterministic, as nearly all nodes recover after one time step. For low values of p , the nodes recover from the refractory state after longer times. We previously observed for the deterministic node dynamics ($p = 1$) that the network dynamics can settle into a regular oscillatory collective behavior after a transient period [18]. For initialization, we consider a distribution of E, S, R randomly generated, with probability 0.1 to set a node into the excited state E , while the remaining nodes were partitioned into susceptible S and refractory R states. This particular type of initialization containing refractory nodes allows us to break the inherent symmetry present in undirected cycles. Whereas both forward and backward propagation are possible when introducing an excitation in a cycle of susceptible nodes, triplets of neighbors with the initial setting SER induce directionality in the excitation propagation in the cycle. More generally, the refractory state following excitation prevents backward propagation.

B. Network model

As a graph model we consider the classical Erdős-Rényi (ER) random graph [17]. Because the computation of all cycles in dense graphs was not practically feasible, we focused on sparse graphs, with 50 nodes and 60 undirected connections, which corresponds to an average number of neighbors $\langle k \rangle = 2.4$. The networks were generated with the NETWORKX [19] software package, and we kept only fully

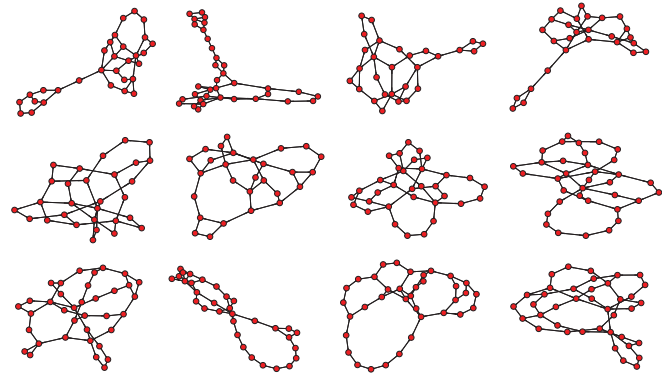


FIG. 1. (Color online) Examples of ER random graphs used in the study, after pruning their dangling ends. These examples are ordered according to the average cycle length, from values close to 11 up to 20, from left to right and top to bottom. Note that short cycles can be embedded in longer cycles.

connected realizations. The list of cycles (that is, closed paths) was obtained with an algorithm developed in [20], which is also implemented in NETWORKX. With the above parameters, the networks are not far from the percolation threshold (see, e.g., [21]). The typical cycle length distribution, averaged over several network realizations, has a Gaussian shape with an average of about 16 (and values ranging from 8 to 20) and standard deviation of about 2. While in many cases the cycle length distributions had a broad unimodal shape, considerable variation was encountered in individual graph realizations, including cases with no discernible peak or even approximately bimodal shapes. In order to more clearly observe the cycle structure of these graphs and its influence on the excitable dynamics, we iteratively pruned the networks, eliminating all nodes with degree 1 and their links, until all nodes in the networks had a degree equal or greater than 2. These networks have the same number of cycles as the original ones. In Fig. 1 we illustrate nine of these networks ordered by the average cycle length.

C. Measuring cycling excitation

At the core of our investigation is an algorithm for detecting successfully used cycles in an excitation pattern (i.e., in the time series of excitations at each node of the graph). A cycle of length L (L -cycle) consisting of nodes j_1, j_2, \dots, j_L , where each j_i is a node number, is considered to be “successfully used,” when the excitation pattern shows the sequence $j_1, j_2, \dots, j_L, j_1$ as subsequent excitations. We also allow for two simultaneous excitation “waves” on a cycle, but disregard “phase slips,” that is, events where one or more nodes are skipped in the sequence due to phase-advanced external excitations entering the cycle [18]. Particularly, we focus on probing the successful usage of cycles with length smaller than 20 nodes, because cycles of longer length are rarely used during complete turns. Details of the algorithm are given in Appendix A.

We define the average number of turns performed by a L -cycle, $\langle N_{\text{runs}}(L) \rangle$, as the average over runs, then over L -cycles, then over the \mathcal{N} network realizations, of the number of complete turns of excitation achieved by a L -cycle i during a

run:

$$\frac{1}{\mathcal{N}} \sum_{j=1}^{\mathcal{N}} \sum_{L\text{-cycle } i} \frac{\langle N_{\text{run}}(j,i) \rangle_{\text{runs}}}{n_j(L)}, \quad (1)$$

where $N_{\text{run}}(j,i)$ is the number of complete excitation turns achieved by the L -cycle i , in the network realization j , during the considered simulation run, and $n_j(L)$ is the total number of L -cycles in the network realization j .

We also introduce the fraction of time, which L -cycles spend on average in sustaining cycling excitation,

$$L \frac{1}{\mathcal{N}} \sum_{j=1}^{\mathcal{N}} \sum_{L\text{-cycle } i} \left\langle \frac{N_{\text{run}}(j,i)}{T_{\text{run}}} \right\rangle_{\text{runs}}. \quad (2)$$

The ratio $N_{\text{run}}(j,i)/T_{\text{run}}$ is the number of complete turns achieved by the L -cycle i (in the network realization j) divided by the run duration T_{run} . We first average over the runs, then sum over the L -cycles, then average over the network realizations.

D. Mean-field approach of cycling activity

The core of our mean-field approach is to consider a topological cycle within the excitable network (“embedded device”). In standard mean-field excitable dynamics, see Appendix C, the topology of the network is taken into account only through the average degree $\langle k \rangle$. By contrast, our prediction of the activity of a given L -cycle explicitly considers its topology, and follows the cycling excitation along the cycle while considering that the remaining part of the network is in a stationary state of excitation, described by the mean-field excitation density $c^*(E)$, Eq. (C3). The probability $\gamma(L, p)$ of an additional step, once the first turn has been completed in a L -cycle (with dynamics described by a recovery probability p), that is, the probability of a re-excitation of a given node, reads

$$\gamma(L, p) = \sum_{j=1}^{L-2} p(1-p)^{j-1} (1-c^*(E))^{((k)-2)(L-2-j)}. \quad (3)$$

The $c^*(E)$ -dependent factors describe the contribution of the network context, into which the L -cycle is embedded, and ensure that no excitation reaches the site between its recovery (after a variable number j of steps) and the arrival of the cycling excitation wave. The computation yields

$$\begin{aligned} \gamma(L, p) &= \frac{p(1-c^*(E))^{(L-3)((k)-2)}}{1 - \frac{1-p}{(1-c^*(E))^{((k)-2)}}} \\ &\times \left[1 - \left(\frac{1-p}{(1-c^*(E))^{((k)-2)}} \right)^{L-2} \right]. \end{aligned} \quad (4)$$

Note that $\gamma(L=3, p=1) = 1$, as expected. Mean-field computation thus gives the probability that at a given time a L -cycle is active,

$$\gamma(L, p)^L, \quad (5)$$

to be compared to Eq. (2).

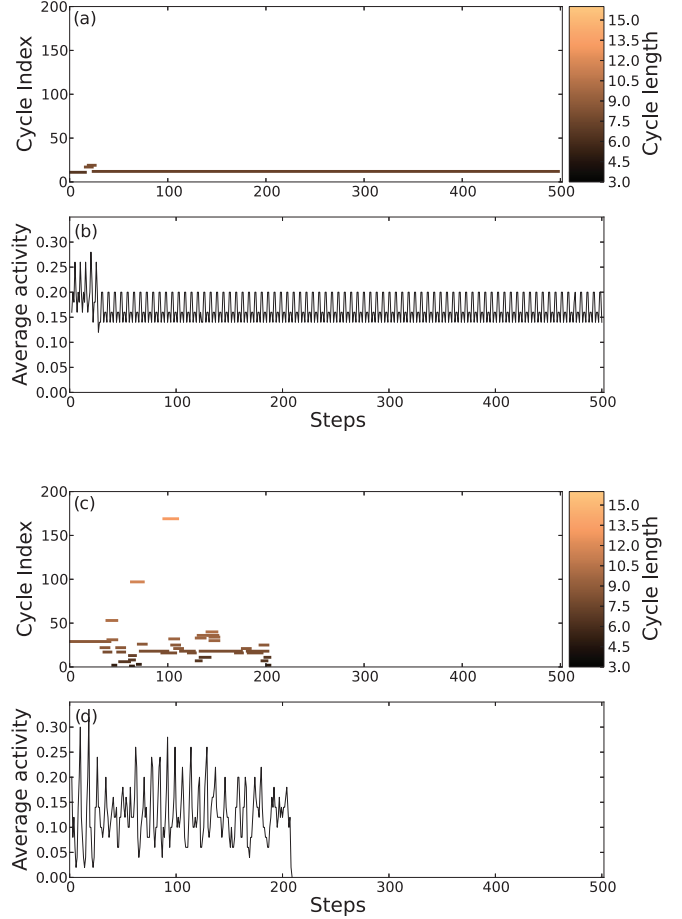


FIG. 2. (Color online) Cycle usage varies qualitatively with the recovery probability. (a) and (c) Cycle usage as a function of time steps, for an ER random network with 50 nodes and 60 links, and two different recovery probabilities. Cycles are sorted by increasing length (cycle index on the left vertical axis) and their length is encoded in color (see the color bar). The initial conditions are the same for both simulations (see text) and the first 10 steps are discarded. The recovery probability is $p = 0.9$ in (a) and (b), and $p = 0.4$ in (c) and (d). (b) and (d) Average activity (total number of nodes in the active state at a given time divided the total number of nodes) as a function of time steps for the same network and initial conditions as in (a) and (c). To present a clear image we only draw the shortest 200 cycles (the other, longer, cycles were not used in complete turns in this case).

III. RESULTS

A. Cycle usage

In order to investigate the dynamic usage of cycles in networks, we ran the excitable dynamic model described above in sparse ER random graphs, and counted the cycles that were used during different runs. Figure 2 shows typical runs of the dynamics for two different values of the recovery probability. At high p [Fig. 2(a)], few short cycles are used to sustain the activity of all nodes in the network until the end of the simulation (500 steps). This picture changes significantly with variations of the recovery probability p . Figure 2(c) shows, for the same network and initialization, the cycles that were used for $p = 0.4$: More cycles of longer length are used, but for short periods of time, until the excitation

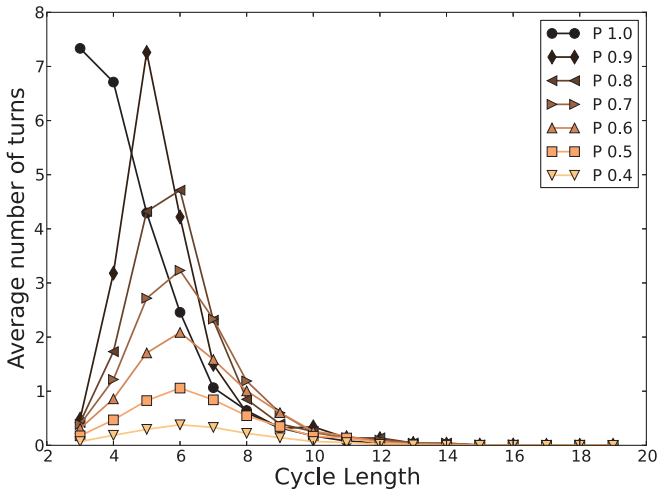


FIG. 3. (Color online) Trade-off between cycle recoverability and vulnerability to external excitations. The figure displays the average number of complete excitation turns achieved by L -cycles, Eq. (1) as a function of their length L . The average is performed over simulation runs (200 different initial conditions), then over L -cycles, then over 100 network realizations.

dies out before the end of the simulation. Consistently, for p close to one, very few short cycles are persistently used and enslave all the other nodes in the graph. By contrast, for small values of p , a vast number of cycles of different lengths are used for relatively short periods of time, and in this way sustained activity is achieved. It is known that the parameter p varies both the average ($1/p$) and the standard deviation ($\sigma = \sqrt{1-p}/p$) of the refractory time distribution. It is noteworthy that this variation translates into a more diverse cycle usage, as observed in Fig. 2(c). First, refractory time obviously constrains the minimal time interval between successive excitations of a given node, hence the length of cycles is relevant. For instance, for a constant refractory period of one, the smallest cycles that can be used are cycles of length 3 [18]; for a constant refractory time of two, the smallest device that can produce sustained activity are cycles of length 4, and so on. In the case of a probabilistic recovery, the fact that longer cycles are used when the average refractory time is increased can be seen in the average number of turns of cycles of length L (Fig. 3). Furthermore, when the recovery probability is close to one, shorter cycles are more often used and this usage is for longer periods of time (more turns per cycle), while a decrease in the recovery probability results in longer cycles being used, for short periods of time. Each simulation corresponds to a different initial condition, that runs for a maximum number of 500 steps. The increase in the dispersion of the refractory times contributes to disrupting the usage of cycles, so that the activity can be maintained only if other cycles are involved. For example, if a node that belongs to a pacemaker cycle of length 3 cannot be recovered after one time step, the activity of the cycle will be abolished in the following steps, and, if other cycles cannot be recruited to ensure propagation of the excitation, network activity will die out. Consequently, the average number of cycles used per run increases when the recovery probability decreases

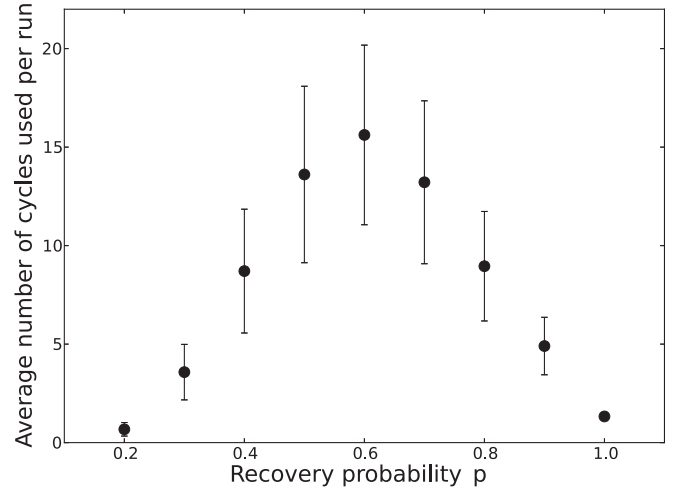


FIG. 4. Trade-off between average lifetime decrease (at low p) and disruption of short cycles (at high p). The figure displays the average number of L -cycles used per simulation run as a function of the length L , for various recovery probabilities p . The average is performed over simulation runs (200 different initial conditions), then over L -cycles, then over 100 network realizations. Error bars correspond to the dispersion observed across network realizations.

up to a recovery probability of 0.6, where the number of used cycles reaches a maximum value, indicating a trade-off effect. This effect is summarized in Fig. 4. By increasing the dispersion further, fewer cycles can be used per run, decreasing the average lifetime of the network. We confirmed this hypothesis with a modified model that keeps the dispersion constant, while the average refractory time is increased (view Appendix B).

B. Comparison between the simulation and the mean-field predictions

At this stage, both simulation results and mean-field predictions evidence a low usage of long cycles (see Figs. 5

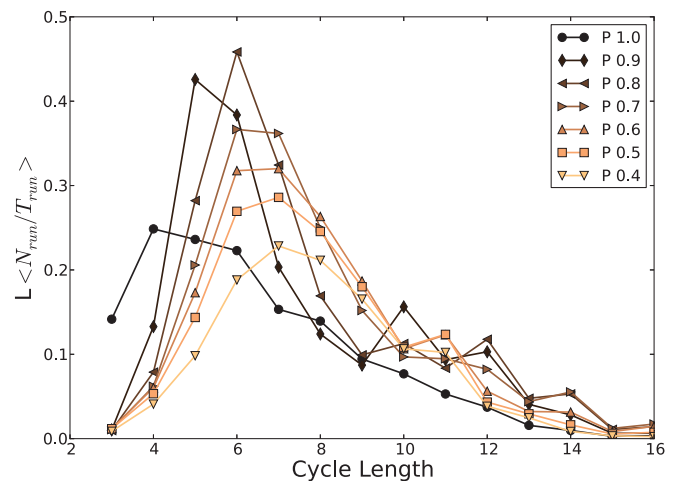


FIG. 5. (Color online) Cycle usage observed in the simulation. The figure displays Eq. (2), as a function of the cycle length, for various recovery probabilities p .

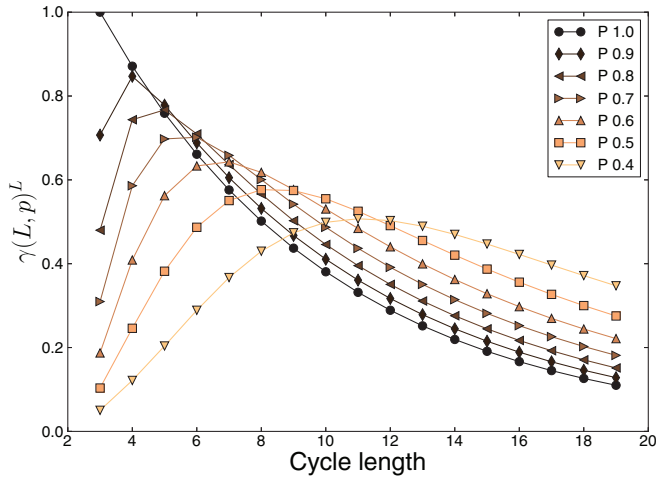


FIG. 6. (Color online) Cycle usage predicted by the mean-field approach. The figure displays the mean-field prediction for $\gamma(L, p)^L$, Eq. (5), as a function of the cycle length, for various recovery probabilities p .

and 6). Nonetheless, we continued to investigate the functional role of long cycles in excitable dynamics, and showed that long cycles make a significant contribution to the lifetime of self-sustained network activity.

By comparing Figs. 5 and 6, taking into account the mechanisms incorporated in the mean-field model, we can thus qualitatively understand the peaklike behavior of the cycle usage as a function of the cycle length. The mean-field model incorporates the two competing effects discussed above: Starting from $p = 1$ (where cycles of length 3 contribute the strongest to cycle usage), at decreasing p ever longer cycles dominate the cycle usage. However, the vulnerability to random excitations also increases with cycle length, thus reducing the amplitude of the peaks.

In addition to the qualitative agreement between the numerical results (Fig. 5) and the mean-field result (Fig. 6), we can also discern a dramatic difference: The mean-field model considers cycles *in isolation*; the effect of the rest of the network is emulated by random (external) excitations. In the numerical simulations, however, we observe that a long successful usage of one cycle tends to suppress the usage of other cycles. In [18] we have investigated in detail, how (in the deterministic limit of the model) a period-3 cycle can enslave the rest of the network into a periodic response. For the more general case (stochastic model, longer cycles) explored here, Fig. 2 shows some numerical evidence for this enslavement: At high p [Figs. 2(a) and 2(b)] only a single cycle is used across a large time window; but even at lower p [Figs. 2(c) and 2(d)], in spite of the very large number of cycles being used in total, in most small time windows only one or two cycles are used simultaneously.

In the following, we will provide ample numerical evidence, that long cycles, in spite of their rare usage, are *functionally* important for maintaining activity in the network. We start by showing that a higher average cycle length in the network means a longer average lifetime of excitation. It is clear, however, that an aggregated topological quantity like the average cycle length does not directly hint at the mechanisms

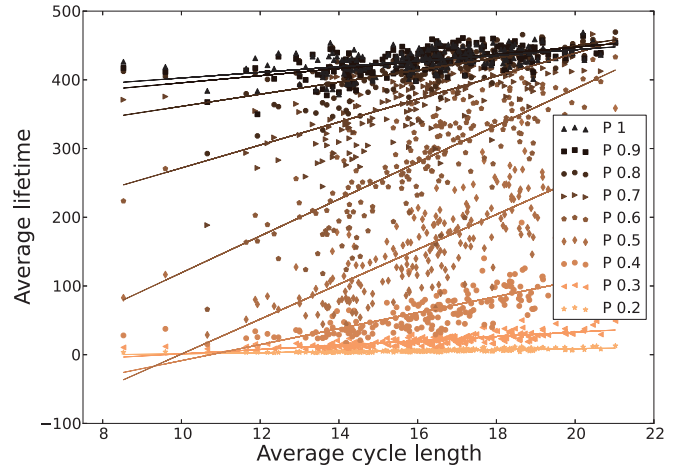


FIG. 7. (Color online) Lifetime of the excitable dynamics varies with the average length of a topological cycle. The figure displays the average lifetime of the network activity for different values of the recovery probability p , as a function of the average cycle length in the graph. The average lifetime was computed running 200 different initial conditions for each network, and we here present for each value of p a scatter plot for 200 network realizations.

underlying its impact on the dynamics. We continue by systematically studying the usage of long cycles and show that (1) the longer the cycles being used, the larger is the lifetime of excitations, and (2) strengthening long cycles (by cutting shortcuts through such cycles) enhances lifetime.

C. The impact of cycles on self-sustained network activity

We now turn from the scale of individual cycles in the network to self-sustained activity in the network as a whole. In particular, we want to understand the impact of the cycle length distribution in a graph on the sustainability of the network activity. We thus investigated the average lifetime of network activity (average over a fixed number of initial conditions) as a function of the average cycle length of each network (Fig. 7). We found that networks with larger average cycle length live longer on average, independent of the recovery probability. (The average cycle length shows the clearest correlation with the average lifetime, but weak correlations are also observed for two other characteristics of the cycle length distribution; see Appendix D). The distribution of cycle lengths in the network has the strongest impact on the dynamics of the global network activity for values of p in the range $p \in [0.5, 0.7]$. More cycles are needed per run to maintain the activity of the network in this dynamical regime (Fig. 4); therefore the average cycle length in the network plays a key role. When p is close to one or close to zero, fewer cycles are used per run, therefore the cycle composition of the graph does not have a strong effect on the average lifetime. In this relationship between average lifetime and average cycle length, the extreme cases in p are easy to understand: For very high p , the activity of a few used short cycles cannot be disrupted while the rest of the network is enslaved by these pacemakers (see Fig. 7; see also [18]). Thus, the average lifetime is high irrespective of the average cycle length; consequently, only a weak dependence (low slope in Fig. 7) is observed. At very low p , the average lifetime of

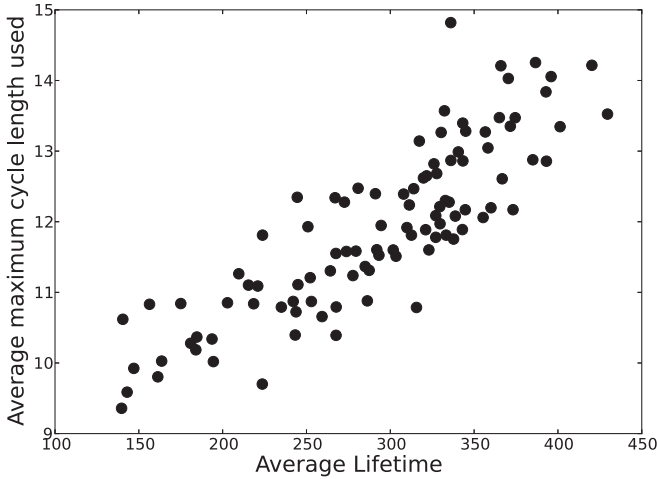


FIG. 8. Long excitation lifetime correlates with usage of long cycles. The figure displays the average maximum length used for each network realization and the corresponding average lifetime (average over runs for both the maximum length and lifetime, scatter plot over 100 network realizations). The recovery probability is $p = 0.6$.

activity is short, and again independent of the cycle content of the graph. Therefore, also in this case a low dependency of activity on cycle length is seen in Fig. 7. At intermediate values of p , by contrast, the cycle content of the graph has a very strong influence on the average lifetime (high slope) and we observe a strong interdependence of the two quantities. In the subsequent investigation, we focus on this intermediate regime and particularly consider $p = 0.6$.

In the following, we show that the increase in the average lifetime of activity is caused by longer cycles being used for longer time in networks with large average cycle length. Longer cycles are more robust against recovery failure of the nodes in a cycle (i.e., nodes still being refractory when the cycling excitation reaches them and thus preventing subsequent successful cycle use), due to the simple fact that each node has more time to recover. To this end, we compute for each network realization two quantities: the average maximum cycle length used in a run (average over runs, Fig. 8) and the sum of the average number of complete turns (average over runs) of all cycles of length smaller than 7 (S_1) and equal or greater than 7 (S_2) multiplied by the length of the cycle (Fig. 9),

$$S_1 = \sum_{\text{cycles } i \text{ of length } L_i < 7} \langle N_{\text{run}}(i) \rangle_{\text{runs}} \times L_i, \quad (6)$$

and

$$S_2 = \sum_{\text{cycles } i \text{ of length } L_i \geq 7} \langle N_{\text{run}}(i) \rangle_{\text{runs}} \times L_i, \quad (7)$$

where $N_{\text{run}}(i)$ denotes the number of complete turns of excitation achieved by the cycle i during the considered simulation run. These complete turns are not necessarily consecutive. These quantities S_1 and S_2 provide the average number of steps spent under the form of cycling excitation (complete turns, average over runs) in each length class, respectively, $L < 7$ and $L \geq 7$. They can, thus, be interpreted as the contributions to the average lifetime of cycling excitation in either short or long cycles. Both the maximum

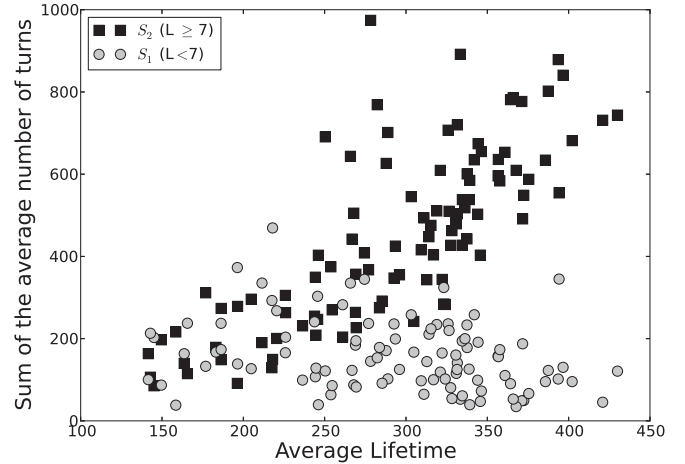


FIG. 9. Usage of long cycles is functionally essential. The figure displays the sum of the average time $L \langle N(L) \rangle_{\text{runs}}$ spent in cycling excitation over cycles of length L smaller than 7 (S_1 , light gray dots) and equal or greater than 7 (S_2 , black squares), and the corresponding average lifetime (average over runs, scatter plot for 100 network realizations). The recovery probability is $p = 0.6$.

length (Fig. 8) and the time spent in long cycles (S_2 in Fig. 9), increase with average lifetime, whereas the time spent in short cycles (S_1 in Fig. 9) is relatively constant.

D. The role of shortcuts in cycles

As a next step, we wanted to understand what specific topological properties of long cycles are relevant for the observed impact on the average lifetime of excitable dynamics. The most conspicuous property we identified was a substructure in terms of shorter cycles. We, therefore, focused on the role of shortcuts, that is, single edges between two nodes of a long cycle producing two embedded shorter cycles. A shortcut in a cycle can spread the excitation in both directions, annihilating excitations moving along one direction, and disrupting the sequential activation of the cycle. Thus, one may hypothesize that cycles without shortcuts are used more frequently. This hypothesis is confirmed by Fig. 10. An additional confirmation of the hypothesis comes from analyzing how the elimination of shortcuts in cycles can modify the average lifetime of a network. A common view on such shortcuts is that they tend to facilitate self-sustained activity (see, e.g., [3]). Also, eliminating shortcuts will reduce the number of short cycles, thus depriving the network of potential pacemakers. In contrast to this view, we found that cutting shortcuts of long cycles increases the average lifetime of network activity (see Fig. 11). This result agrees with our hypothesis that longer cycles are more robust against failures coming from the nonrecovery nodes. Statistical evidence points to a marginal role of long cycles in excitable dynamics (cf. Figs. 3 and 5). However, use of long cycles, although rare, appears to be functionally essential for sustaining activity. As a final step, we closely studied individual cases, in order to arrive at a more mechanistic understanding of the role of long cycles. We investigate the edges of cycles that were used most frequently (within complete turns) for a recovery probability $p = 0.6$ [see Fig. 12(a)]. Then, we cut one of these edges

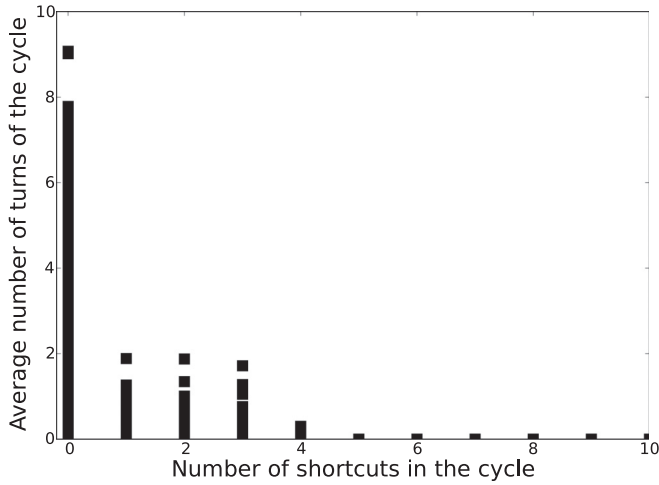


FIG. 10. Shortcuts hinder or reduce long cycle usage. Average number of complete excitation turns (over runs) achieved by a cycle as a function of the number of shortcuts present in the cycle (scatter plot for 100 network realizations and all their cycles). The recovery probability is $p = 0.6$.

and reran the simulations with the modified network, and finally computed as before the average lifetime of the modified networks. In Fig. 11, we display a histogram of the number of cut edges that increase the average lifetime divided by the total number of edges cut (for edges that are shortcuts and nonshortcuts).

In conclusion, we have developed an algorithm to identify the different cycles that are used in networks of excitable discrete dynamics. We are able to detect the dynamical pacemaker loops at different times in a run. Moreover, we have studied the main features of the cycle length distribution that affect the average lifetime of a network. We observed that graphs with larger average cycle length live longer on average, due to the presence and use of long cycles. This observation

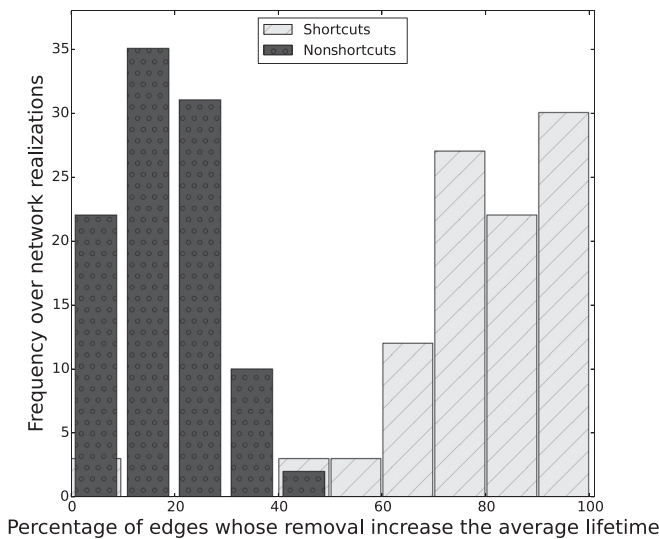


FIG. 11. Removal of shortcuts increases the lifetime. Histogram (over 100 network realizations and over 2000 initial conditions) of the percentage of edges among shortcuts (light gray) or nonshortcuts (black), whose removal increases the average lifetime.

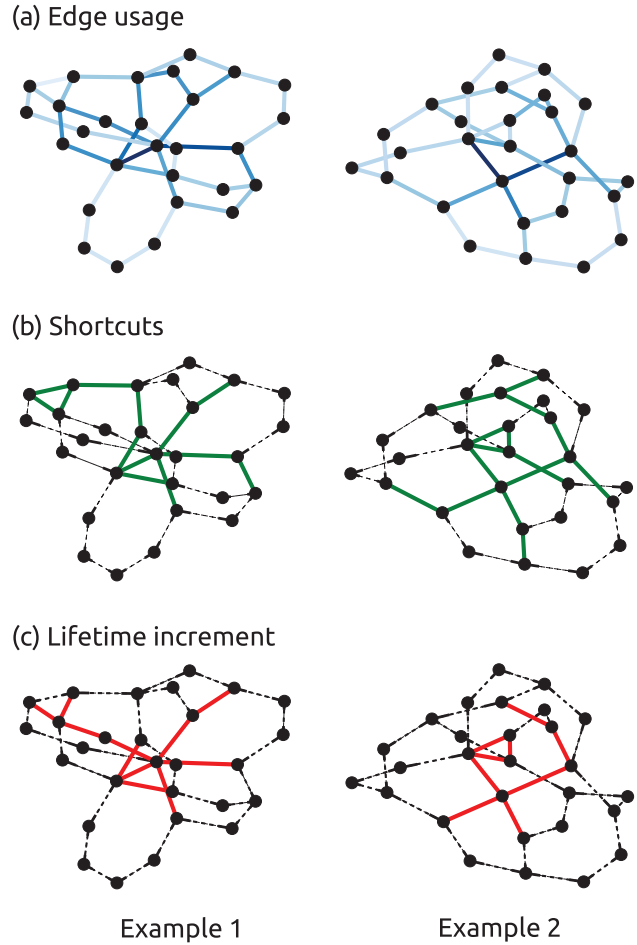


FIG. 12. (Color online) Dynamical features of excitable networks and their topological determinants. Representation of (a) edge usage, with edge darkness increasing with its usage, (b) shortcuts of cycles (green edges), and (c) edges whose removal produce an increase of the average lifetime when rerunning the simulation (in red).

is also linked to the role of shortcuts in cycles, as eliminating shortcuts of long cycles in a graph can increase the transient length of excitation patterns and, thus, positively contributes to self-sustained network activity.

IV. DISCUSSION

In previous work, the role of cycles in excitation propagation could only be assessed indirectly, for instance, by pruning the network based on dynamic information in order to identify the most relevant cycles. Here, we use a minimal three-state model of excitable node dynamics, which allowed a direct and unambiguous algorithmic definition of a successfully used cycle, and provided a basis for studying the contributions of cycles of any length in a network. To our knowledge, this is the first time that the impact of long cycles on network activity has been analyzed.

The analyses provided several new insights. It has been pointed out before that short cycles can have an amplifying role for excitable dynamics [18]. The surprising new finding is the systematic impact long cycles [28] have on sustained

activity. We provide a detailed topological characterization of long cycles, which extend the average lifetime of network activity by implementing a storing capacity for excitations. This effect was also demonstrated by removing the shortcuts in long cycles, which resulted in an extended lifetime. Focusing on individual links in the network, three properties were often observed together: (1) A link was frequently used, that is, it was situated in one or several frequently used cycles; (2) a link was a shortcut in a longer cycle; (3) removing the link increased the average lifetime of network excitation.

Putting all these results together, we come up with a very clear general picture, how the cycle content of a graph influences self-sustained activity:

(1) The length of the largest cycle successfully used is a good predictor of the transient length (Fig. 8); usage of long cycles is thus associated with the sustainment of activity.

(2) Usage of cycles longer than (approximately) $1/p$ correlates with the lifetime of excitations, while no such correlation is observed for shorter cycles (Fig. 9).

(3) When cutting shortcuts in long cycles, the average lifetime increases significantly (Fig. 11).

Typically, links that are shortcuts within long cycles unite two interesting dynamical properties: They are particularly often used in successful turns and cutting them increases the mean lifetime (Fig. 12). A clear hierarchy of links is thus established in the network with respect to their importance for sustained activity. Long cycles are instrumental in establishing this hierarchy.

Our findings draw attention to the cycle content of a graph, as an important topological property underlying pattern generation [22], re-entry [23], and iterative signal processing [24]. While the impact of short cycles has been explored from diverse angles in previous studies, we here emphasize that the successful usage of long cycles can be instrumental in maintaining activity in a network of excitable units. Even though it is still computationally challenging to enumerate cycles in larger networks, it will be fascinating to see whether some selective pressure may act on real neural networks enhancing their inventory of long cycles.

The fact that long cycles were of such prominent importance for the average lifetime of excitations and, therefore, constitute a topological feature enhancing self-sustained activity, can be expected to be a universal phenomenon of excitable dynamics on graphs. However, it is currently unknown how our findings and the global picture derived from them extend to larger and denser graphs, such as excitable brain networks [25–27]. Moreover, it is clear that the cycle composition is one of several topological features of graphs relevant for their dynamic function. We can expect, for example, that the hierarchical organization of a network (i.e., a module-within-module structure) is, qualitatively speaking, responsible for splitting tasks into subtasks, while within each (sub-)module the cycle content may then be of relevance for aspects such as sustaining local dynamics.

ACKNOWLEDGMENTS

Our research has been supported by Deutsche Forschungsgemeinschaft (DFG) Grants No. HU-937/7-1, No. HI 1286/5-1, and No. SFB 936/A1.

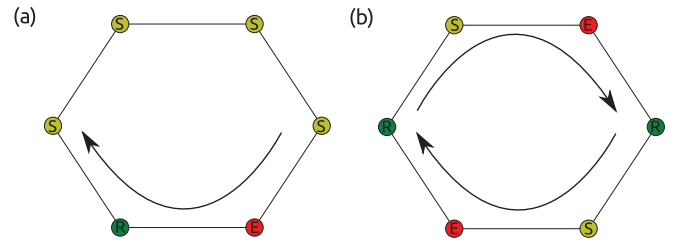


FIG. 13. (Color online) Counting cycling excitation. Schematic representation of one (a) and two (b) excitations traveling through a cycle. Excited nodes (E) are plotted in red, susceptible nodes (S) in yellow, and refractory nodes (R) in green. The arrows indicate the direction of excitation propagation.

APPENDIX A: BRIEF DESCRIPTION OF ALGORITHM TO COMPUTE THE SUCCESSFULLY USED CYCLES

This section describes briefly the implemented algorithm for detecting cycle usage in a graph. The procedure begins by computing the list of all cycles in a graph, using the “simple cycles” routine in NETWORKX [19]. The excitation pattern of each cycle is analyzed for 200 different initial conditions. A L -cycle, composed of nodes j_1, j_2, \dots, j_L and showing the excitation pattern sequence $j_1, j_2, \dots, j_L, j_1$ is considered to be used once. We also allow for two excitation “waves” concurrently traveling on a cycle, as shown in Fig. 13(b). In this case we considered the cycle to be used twice. For each cycle in the network, we analyzed the excitation pattern of its nodes and we created four lists of lists in Python, two containing the sequential activation of the nodes and the other two the respective times of activation. We check the length of the sublists and the time differences within them. We only kept the sublist with length longer than the length of the cycle and with all time differences of one (if the time difference is greater than one, we cut both lists there). Now the sublist of nodes contain sequences of nodes of the same length or longer than the length of the cycle. We finally compared the length of these lists with “multiples” $nL + 1$ of the cycle length L , where n is a natural number. The length of the lists can be equal or greater than these multiples, if they are equal, this means that an excitation has traveled an integer number of times through the cycle; and if the length of the list is between two multiples, the excitation has traveled a noninteger number of times through the cycle. In this case we consider the minimum integer as the number of times the cycle was used in a sequential manner. Indeed, a partial turn (excitations in a row) of a short cycle embedded in a longer one could be confused with a partial turn of the long cycle; this is why we consider only complete turns.

APPENDIX B: MODIFIED MODEL

In order to better understand the interplay of the cycle length distribution with the refractory time distribution, we also employed a family of models M_n , where a refractory element resides in this state for minimally n time steps, before the recovery probability is evoked. In this notation, M_1 is the original model. We analyzed which cycles were used for this family of models. We considered $n = 2, 3, 4$

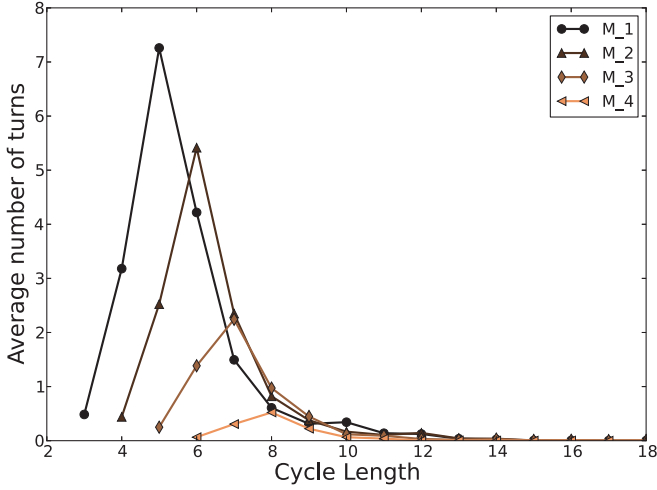


FIG. 14. (Color online) Enhanced refractory period displays the same recoverability/vulnerability trade-off. Average number of turns of L -cycles for the original model M_1 and the modified models M_2 , M_3 , and M_4 , for a recovery probability $p = 0.9$. The number of turns for each network was computed using 200 initial conditions, and the final average was computed over 100 different network realizations [see Eq. (1)].

with recovery probability of 0.9. With the model M_2 , the nodes can have a minimum refractory time of two time steps; therefore, the pacemaker cycles can only have length greater or equal to 4. With the model M_3 the minimum refractory time is 3, so the minimum pacemaker cycles could have length greater or equal to 5, etc. The interest of such models is to monitor independently the average refractory time ($n - 1 + 1/p$) and its standard deviation ($\sigma = \sqrt{1-p}/p$), hence to disentangle their influence onto cycle usage. In Fig. 14, we plot the average number of turns of L -cycles as a function of L for different dynamical parameters and different model realizations. The peak of the curve moves toward long cycles as the minimum refractory period n and the average refractory time increase (at fixed standard deviation).

In the original model M_1 , the increase of the average refractory time $1/p$ is accompanied by an increase of the dispersion of the refractory times, which translates into a broad distribution of refractory times of *cycles* (i.e., the time it takes after a cycle usage, until all nodes have recovered) and, as a consequence, might result in a wider range of cycles being used. In contrast, increasing the average refractory time in the modified model is done by increasing n , at fixed $p = 0.9$ hence at fixed standard deviation ($\sigma = 0.35$).

The modified model allowed us to separately study the effect of the mean refractory time and its standard deviation. In Fig. 15, we compared the average number of cycles used per run (average over runs then over network realizations) as a function of the average refractory time for the original and modified models. We observed that the peak at intermediate refractory times in the number of cycles used was indeed a consequence of the large standard deviation in the minimal model.

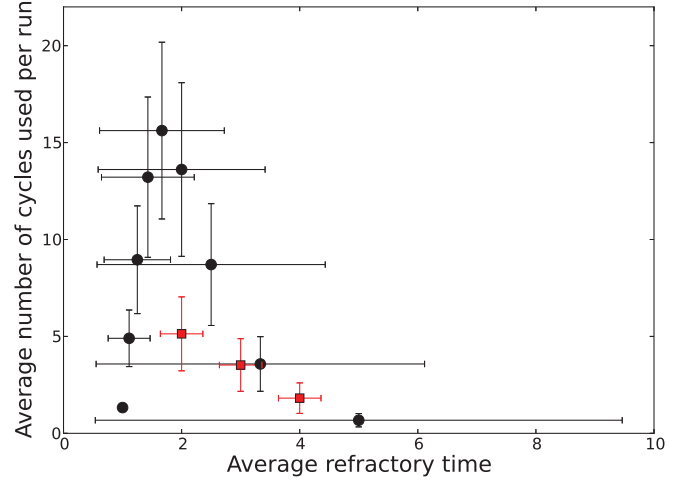


FIG. 15. (Color online) Refractory time dispersion correlates with the number of used cycles. Average number of cycles used per run versus the average refractory time, for the original model (black dots) at increasing average refractory time $1/p$, hence increasing standard deviation $\sigma = \sqrt{1-p}/p$, and the modified model (red squares) for $n = 2, 3, 4$ with $p = 0.9$, hence increasing average refractory time $n - 0.1$ and fixed standard deviation ($\sigma = 0.35$). The average was computed over runs and network realizations. Horizontal error bars display the standard deviation σ of the refractory time, while vertical error bars are computed from the simulation (dispersion over runs and network realizations).

APPENDIX C: MEAN-FIELD APPROACH FOR NETWORK EXCITABLE DYNAMICS

In a mean-field approach, the network dynamics is described in terms of the densities $c(E, t)$, $c(S, t)$, and $c(R, t)$ of states E , S , and R , respectively. The mean-field equations of evolution read

$$\begin{aligned} c(E, t + 1) &= c(S, t)[1 - (1 - c(E, t))^{\langle k \rangle}] \\ c(S, t + 1) &= 1 - c(E, t + 1) - c(R, t) \\ c(R, t + 1) &= c(E, t) + (1 - p)c(R, t). \end{aligned} \quad (C1)$$

The mean-field approximation lies here in the expression $1 - (1 - c^*(E))^{\langle k \rangle}$ for the probability that a node has at least one excited neighbor: It considers that each node has an average number $\langle k \rangle$ of neighbors each having a probability $c^*(E)$ to be excited (hence a probability $1 - c^*(E)$ to be in a nonexcited state). Also, correlations between neighbors are ignored. The topology of the network is taken into account only through the average node degree $\langle k \rangle$. The stationary state $(c^*(E), c^*(S), c^*(R))$ satisfies

$$\begin{aligned} c^*(S) + c^*(E) + c^*(R) &= 1 \\ c^*(R) &= c^*(E)/p \\ c^*(E) &= c^*(S)[1 - (1 - c^*(E))^{\langle k \rangle}]. \end{aligned} \quad (C2)$$

We may determine this stationary solution using the approximation $1 - (1 - c^*(E))^{\langle k \rangle} \approx \langle k \rangle c^*(E)$, which yields

$$c^*(S) = \frac{1}{\langle k \rangle}, \quad c^*(E) = \frac{1 - 1/\langle k \rangle}{1 + 1/p}, \quad c^*(R) = \frac{1 - 1/\langle k \rangle}{p + 1}. \quad (C3)$$

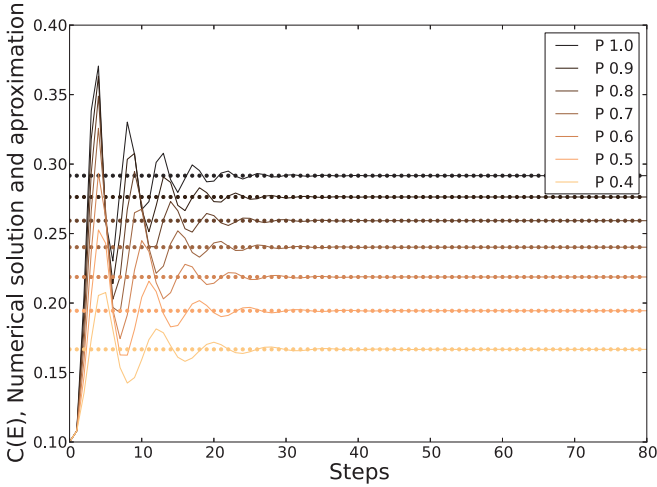


FIG. 16. (Color online) Validation of the approximate solution Eq. (C3). Comparison of the numerical solution of the stationary mean-field equations, Eq. (C2) (continuous line), for the excitation density, and the approximation $c^*(E) = (1 - 1/\langle k \rangle) / (1 + 1/p)$, Eq. (C3) (dotted line), as a function of p , for $\langle k \rangle = 2.4$. Note the scale on the vertical axis.

Interestingly, this approximation of the mean-field excitation density gives very good results for sparse graphs compared to the full solution of the mean-field equations, Eq. (C1), as shown on Fig. 16. We perform a “second-order mean-field computation,” plugging the stationary mean-field densities ($c^*(S), c^*(R), c^*(E)$) in an analysis of the excitation of topological cycles and associated combinatorics. More specifically, we consider a L -cycle, embedded in a network in the mean-field stationary state ($c^*(S), c^*(R), c^*(E)$). We adopt a moving view, computing the probability that each successive node is in the proper state when excitation arrives, which yields Eq. (3).

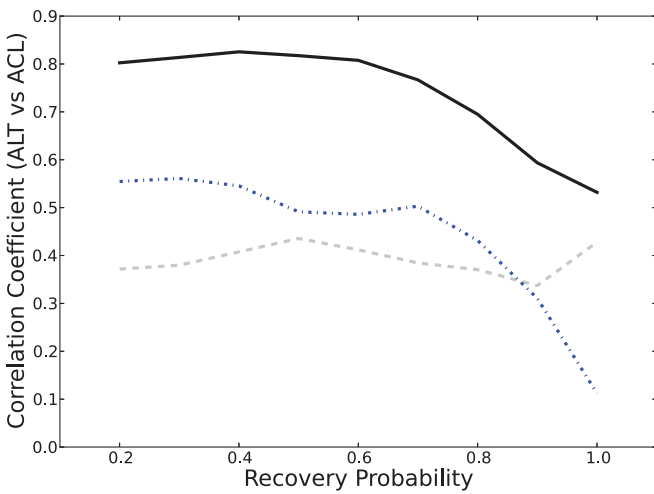


FIG. 17. (Color online) Among the features of the cycle length distribution, lifetime correlates best with the average cycle length. Correlation coefficient of the average lifetime with the average cycle length (full black line), with the total number of cycles (dash-dotted blue line), and with the standard deviation of the cycle length distribution (dashed gray line) for different recovery probabilities.

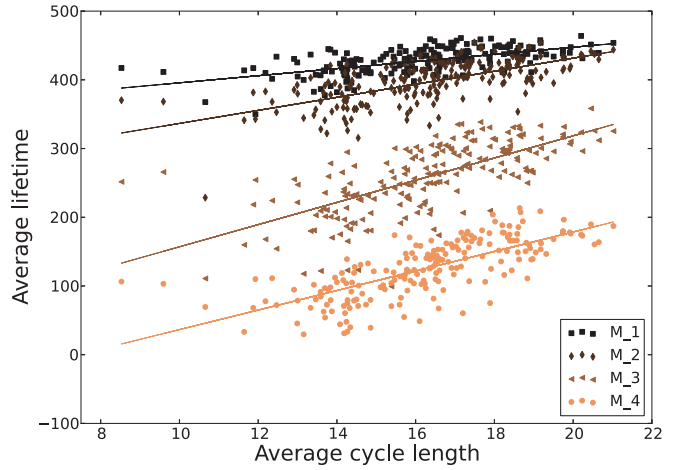


FIG. 18. (Color online) Dependence of the average lifetime on the average cycle length for the modified model. Average lifetime of the network activity for different model realizations (200 different initial conditions for each network, and 200 different network realizations) as a function of the average number of cycles in the graph, for the four models $M_n, n = 1, 2, 3, 4$.

In this formula, all the nodes of the cycle are considered to have a degree equal to the average value $\langle k \rangle$. If necessary, formula Eq. (3) easily extends to account for a given sequence of degrees for the cycle nodes.

APPENDIX D: AVERAGE LIFETIME

While the average cycle length shows the strongest correlation to the average lifetime (Fig. 17, full black line), similar correlations are also observed for the total number

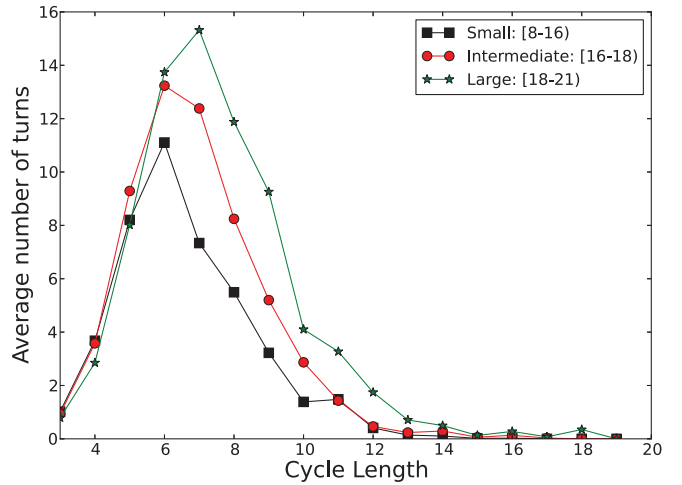


FIG. 19. (Color online) Trade-off between cycle recoverability and vulnerability to external excitations. The figure displays the average number of complete excitation turns achieved by L -cycles, Eq. (1) as a function of their length L . The average is performed over simulation runs (200 different initial conditions), then over L -cycles, then over network realizations. The networks were grouped in three classes according to their average cycle length (L): small, $8 \leq \langle L \rangle < 16$, 40 networks; intermediate, $16 \leq \langle L \rangle < 18$, 35 networks; large, $18 \leq \langle L \rangle < 21$, 25 networks.

of cycles in the graph (Fig. 17, dash-dotted blue line) and for the standard deviation of the cycle length distribution (Fig. 17, dashed gray line). Additionally, we compared in Fig. 18 the dependence of the average lifetime as a function of the average cycle length for the modified model. Since all the models use on average a similar amount of cycles per run, we expected to observe a similar slope for all the models, in contrast to Fig. 7, which is actually the case. In order to arrive at an even clearer mechanistic picture according to which the correlation between the average cycle length and the average lifetime (Fig. 7) is, indeed, due to an increased

usage of long cycles, we performed the following additional investigation: We grouped networks in three classes, according to their average cycle length $\langle L \rangle$ (small, $8 \leq \langle L \rangle < 16$, 40 networks; intermediate, $16 \leq \langle L \rangle < 18$, 35 networks; large, $18 \leq \langle L \rangle < 21$, 25 networks) and computed the corresponding curve (see Fig. 19, average number of turns as a function of cycle length; $p = 0.6$) from Fig. 3 for these groups separately. It is clearly seen that usage of longer cycles is enhanced in networks with a larger average cycle length $\langle L \rangle$. Figure 19 interlinks our two key observations: the cycle usage curves and the impact of the average cycle length on excitation lifetime.

-
- [1] I. Timofeev, M. Bazhenov, J. Seigneur, and T. Sejnowski, *Neuronal Synchronization and Thalamocortical Rhythms in Sleep, Wake and Epilepsy* (Oxford University Press, Oxford, 2012).
- [2] T. Lewis and J. Rinzel, *Netw. Comput. Neural Syst.* **11**, 299 (2000).
- [3] A. Roxin, H. Riecke, and S. A. Solla, *Phys. Rev. Lett.* **92**, 198101 (2004).
- [4] X. Liao, Y. Qian, Y. Mi, Q. Xia, X. Huang, and G. Hu, *Front. Phys.* **6**, 124 (2011).
- [5] Y. Qian, X. Huang, G. Hu, and X. Liao, *Phys. Rev. E* **81**, 036101 (2010).
- [6] P. McGraw and M. Menzinger, *Phys. Rev. E* **83**, 037102 (2011).
- [7] N. Vladimirov, Y. Tu, and R. D. Traub, *Front. Comput. Neurosci.* **6**, 17 (2012).
- [8] S. Bornholdt, *Science Signaling* **310**, 449 (2005).
- [9] R. Pastor-Satorras and A. Vespignani, *Phys. Rev. Lett.* **86**, 3200 (2001).
- [10] S. Wolfram, *Rev. Mod. Phys.* **55**, 601 (1983).
- [11] L. A. N. Amaral, A. Díaz-Guilera, A. A. Moreira, A. L. Goldberger, and L. A. Lipsitz, *Proc. Nat. Acad. Sci. USA* **101**, 15551 (2004).
- [12] C. Marr and M. Hütt, *Physica A* **354**, 641 (2005).
- [13] C. Marr and M. T. Hütt, *Phys. Lett. A* **373**, 546 (2009).
- [14] A. A. Moreira, A. Mathur, D. Diermeier, and L. A. N. Amaral, *Proc. Natl. Acad. Sci. USA* **101**, 12085 (2004).
- [15] C. Marr and M. T. Hütt, *Phys. Lett. A* **349**, 302 (2006).
- [16] S. Wolfram, *Physica D* **10**, 1 (1984).
- [17] P. Erdős and A. Rényi, *Publ. Math. Inst. Hung. Acad. Sci.* **5**, 17 (1960).
- [18] G. Garcia, A. Lesne, M. Hütt, and C. Hilgetag, *Front. Comput. Neurosci.* **6**, 50 (2012).
- [19] A. A. Hagberg, D. A. Schult, and P. J. Swart, in *Proceedings of the 7th Python in Science Conference (SciPy2008)* (SciPy, Pasadena, 2008), pp. 11–15.
- [20] D. B. Johnson, *SIAM J. Comput.* **4**, 77 (1975).
- [21] R. Albert and A.-L. Barabasi, *Rev. Mod. Phys.* **74**, 47 (2002).
- [22] R. Pan and S. Sinha, *Europhys. Lett.* **85**, 68006 (2009).
- [23] G. M. Edelman and J. A. Gally, *Front. Integr. Neurosci.* **7**, 63 (2013).
- [24] O. Sporns, G. Tononi, and G. M. Edelman, *Cereb. Cortex* **10**, 127 (2000).
- [25] J. W. Scannell, G. A. Burns, C. C. Hilgetag, M. A. O’Neil, and M. P. Young, *Cereb. Cortex* **9**, 277 (1999).
- [26] P. Hagmann, L. Cammoun, X. Gigandet, R. Meuli, C. Honey, V. Wedeen, and O. Sporns, *Plos Biol* **6**, e159 (2008).
- [27] N. Markov, M. Ercsey-Ravasz, A. Ribeiro Gomes, C. Lamy, L. Magrou, J. Vezoli, P. Misery, A. Falchier, R. Quilodran, M. Gariel *et al.*, *Cereb. Cortex* **24**, 17 (2014).
- [28] In this context, terms such as ‘short’ and ‘long’ cycles may appear somewhat arbitrary. A plausible reference for the cycle length is the integer closest to $1/p + 2 + \sigma$, where $1/p$ is the average refractory period, and $\sigma = \sqrt{1-p}/p$ is the standard deviation of the refractory time. This reference length is 5 for a recovery probability of 0.6.